Direct Observation of Mercury Amalgamation on Individual Gold Nanorods Using Spectroelectrochemistry

*Carola Schopf, Amélie Wahl, Alfonso Martín, Alan O'Riordan, Daniela Iacopino**

Tyndall National Institute, Dyke Parade, Cork, Ireland

Abstract

We report on the use of a spectroelectrochemical method for the investigation of mercury amalgamation on gold nanorods. Hg^{2+} was electrochemically reduced at gold nanorod electrodes and the consequent optical changes resulting from deposition of mercury were monitored by darkfield microscopy. Nanorods displayed marked scattering color transitions from red to green and longitudinal surface plasmon resonance (LSPR) blue shifts up to 197 nm. Corresponding cathodic voltammograms showed strong reduction peaks at potentials which were attributed to Hg^{2+} reduction. The highest optical blue shifts were observed for working electrodes constituted by well-separated gold nanorods deposited on ITO substrates, which also showed transition from diffusion-limited to steady-state electrochemical behavior. Theoretical simulations were carried out to support experimental results and to obtain further insight on the diffusional behavior of mercury reduction at nanorod electrodes. Real time observation of the amalgamation process was performed by monitoring the evolution of spectral response from single nanorods in presence of

Hg^{2+} and subjected to either linear sweep voltammetry or chronoamperometry. The analysis confirmed a direct correlation between the occurrence of spectral changes and the formation of an amalgam resulting from deposition and subsequent diffusion of reduced mercury into the nanorods. This work shows the potential of this method for elucidation of reaction mechanisms occurring at nanoscale electrodes and for sensitive detection of mercury for environmental applications.

Introduction

Direct observation of chemical reactions occurring on the surface of metal nanoparticles is fundamentally important for better understanding of these processes towards nanoparticle-based sensing and catalytic applications. In the last 20 years many research groups have used dark field microscopy to investigate chemical processes occurring on single nanoparticles of various shapes and types.[1-4] This technique pioneered by Klar *et al*.[5] and Schultz *et al.*[6] enables the spectra of the light scattered by single nanoparticles to be measured routinely and to correlate the obtained optical response to nanoparticle morphology. In addition, darkfield microscopy allows direct observation of chemical processes occurring on single nanoparticles, which is greatly helpful for the elucidation of reaction mechanisms at nanoscale. This concept was elegantly demonstrated by Novo *et al.* who investigated nanoparticle-catalyzed oxidative processes at single nanoparticle level by a combined dark-field microscopy-surface plasmon spectroscopy method.[7] The growth of gold nanorods caused by ascorbic acid was monitored through the spectroscopic changes occurring at nanoparticle surfaces, which in turn allowed first time direct observation of chemical reactions under quantum regimes. A further development was proposed more recently by the same authors, consisting in incorporation of electrochemical cells into the darkfield setup in order to enable optical investigation of electrochemical processes occurring on nanoparticle

surfaces.[8] In this spectroelectrochemical approach electrodes constituted by low density nanoparticles deposited on indium tin oxide (ITO) substrates were used to inject electrons into nanoparticles whose optical response was then monitored by darkfield microscopy. In fact, according to the charge density tuning model, changes in charge density affect the bulk plasma density of the metal, resulting in blue shifts of the surface plasmon resonance.[9-10] Therefore, the optical properties of single gold nanorods were modulated using electrochemical charge injection, opening up routes for reaction mechanisms of redox reactions to be studied under quantum catalysis regime (one electron at a time).[8] In another work, Chirea *et al*. used real time spectroelectrochemistry to study the underpotential deposition of silver onto single gold nanostars deposited on ITO substrates.[11] Selective deposition of silver occurred on the surface of gold nanostars allowing the scattering spectrum of resulting core-shell structures to be tuned over 100 nm with deposition of 1-5 nm of silver. This preliminary work culminated in a recent publication where spectroelectrochemistry was used to modulate transitions between capacitive and conductive coupling regimes in gold/silver nanoparticle dimers and to get insights into the reaction kinetics and evolution of the charge transfer plasmon mode of such electrochemically tunable structures.[12]

Recently, our group has used darkfield microscopy to investigate the mechanism of mercury amalgam formation on single gold nanorods deposited on ITO surfaces.[13] A strong chemical reducing agent was used to promote the reduction of Hg^{2+}, which caused alteration of nanorods' optical properties as result of Hg deposition on nanorods and subsequent amalgam formation. Although nanoscale amalgams were prepared since the early days of colloid science, our results were relevant in view of the recent renewed interest for this research field, propelled by the

potential of gold-amalgam nanocomposites for sensing, environmental and technological applications.[14-15]

In this work we present the first application of spectroelectrochemistry for the investigation of a chemical process such as mercury amalgamation on gold nanorods. The electrochemical reduction of Hg^{2+} was accompanied by remarkable nanorod scattering color transitions from red to green and strong blue shifts of the localized surface plasmon resonance (LSPR) of up to 197 nm. Concomitantly, linear sweep voltammograms obtained at nanorod/ITO electrodes showed reduction of Hg occurring upon application of an appropriate potential window. Low density electrodes constituted by well-separated gold nanorods led to the highest number of reduced mercury atoms/nanorod, resulting in the strongest observed optical blue shifts and generation of current profiles approaching steady-state. Real time spectroelectrochemical observation of the amalgam process allowed identification of two processes occurring at different time scales: mercury deposition on gold nanorod surfaces driven by the application of linear sweep potentials followed by diffusion of mercury in the nanorod lattices. In addition, real-time observation of the process at the mercury reduction potential (chronoamperometry) resulted in generation of steady and highly sensitive optical responses. This initial work is an example of the versatile opportunities offered by spectroelectrochemical approaches for nanoscale chemical analysis and for development of future environmental nanoscale sensors with enhanced sensitivity provided by combined optical/electrochemical outputs.

Experimental Methods

Materials

Tetrachloroauric acid, silver nitrate, sodium borohydride, ascorbic acid, cetyltrimethylammoniumbromide (CTAB), mercury chloride were purchased from Sigma-

Aldrich. All glassware was cleaned with acqua regia prior to nanorod synthesis. Milli-Q water (resistivity > 18 MΩ cm^{-1}) was used throughout the experiments.

Synthesis of gold nanorods

Gold nanorods were synthesized by a combined seed-mediated/overgrowth method described by Marzán *et al.*[16] whereby nanorods of average size 11 ± 2 nm × 41 ± 3 nm were firstly synthesized by seed mediated method and subsequently overgrown to a final mean size of 39 ± 3 nm × 76 ± 3 nm, aspect ratio (AR) = 1.9, by further addition of reducing agent ascorbic acid. The as prepared gold nanorod solution (10 mL) was centrifuged twice to remove CTAB excess and re-dispersed in 10 mL of Millipore water. The final CTAB concentration was kept between 0.1 mM and 0.35 mM. Gold nanorods were deposited on resulting transparent ITO substrates by flow deposition from aqueous solutions ca. 33 pM. Subsequently the substrates were rinsed with 40°C deionized water to remove residual surfactants and dried under a stream of nitrogen.

Fabrication of Working Electrode

Transparent electrodes consisted of glass substrates coated with a 20 nm indium thin oxide (ITO) film modified with gold nanorods. Additionally, a unique pattern of 10 nm deep binary alignment marks was lithographically etched in the ITO layer in order to allow spectroscopic localization of gold nanorods.

Darkfield microscopy

Scattering spectra of individual nanorods were acquired with an inverted IX-71 Olympus microscope with an oil immersion dark field condenser (Olympus U-DCW, 1.4 NA) and 50X objective (Olympus LMPlanFL 50x/0.5 NA). The sample was illuminated with a 100 W halogen

lamp. The light collected by the objective was directed either unto a color CMOS camera (DCC1645C, ThorLabs) for image and video acquisition or onto the entrance of slit of a monochromator (SP-2356, Acton Research) equipped with a thermoelectrically cooled, back illuminated CCD (Spec10:100B, Princeton Instruments) for spectra acquisition. The experiments were performed by first recording an image of the sample with a mirror in the light path of the spectrometer. Once a suitable nanostructure was selected, the mirror was switched with a grating (300 groves mm^{-1}) to disperse the scattered light. An individual spectrum was recorded using an acquisition time of 30 s or continuous spectra acquisition was performed at 1 spectrum/second for real time measurements. The scattering spectra were background corrected by subtracting and dividing by a background scattering spectrum taken from a nearby clean area on the sample. To determine the peak scattering wavelength the spectra were fitted with a Lorentzian function.

Spectroelectrochemical measurements

Spectroelectrochemical experiments were performed using an IVIUM PocketSTAT in a three electrode system, whereby gold nanorod modified ITO coated glass cover slips were used as the working electrode and Pt wires (50 µm in diameter) as counter and pseudo-reference electrodes. A 0.1 M KCl solution at pH 6.5 was used as supporting electrolyte, to which various amounts of $HgCl_2$ were added for the nanorod amalgamation experiments in a custom-made electrochemical cell. For all linear sweep voltammetry measurements potentials were scanned at a rate of 50 mV/s. For chronoamperometry a potential of -0.3 V was applied. Scattering spectra of randomly selected gold nanorods were recorded before and after the electrochemical step or in real time during the electrochemical step. The solution was then exchanged for 0.1 M KCl with added $HgCl_2$ between 2 µM and 5 µM concentrations. Again electrochemical measurements were performed with scattering spectra taken of the same selected nanorods before and after or real

time during the electrochemical step. For background subtraction linear sweep voltammograms obtained in KCl only were subtracted from the respective data obtained in Hg^{2+}-containing electrolyte.

Scanning electron microscopy

SEM images of nanorod working electrodes after spectroelectrochemistry were acquired using a field emission SEM (JSM-6700F, JEOL UK Ltd.) operating at beam voltages of 10 kV.

Finite-element simulations

Analyte concentration profiles for mercury reduction at nanorod electrodes were simulated using the commercial software package Comsol Multiphysics®. These simulations were based on an approach used by Wahl *et al.* for nanoscale electrode arrays.[17]

Results and Discussions

Spectroelectrochemical measurements were performed at gold nanorod/ITO working electrodes with a density of 8 nanorods/100 μm^2 (corresponding to an average inter-nanorod distance of 6 μm) encapsulated in a thin electrochemical cell filled with 5 μM Hg^{2+} solution and 0.1 M KCl supporting electrolyte. The nanorod density was determined by counting the number of nanorods in five 48 μm x 60 μm size SEM images taken at electrode random locations (number of nanorods counted and divided by area analysed). Similarly, the inter-nanorod distance was estimated by averaging the spacing measured between multiple adjacent nanorods from SEM images. Darkfield images were recorded before and after the application of cathodic linear potential sweeps and were correlated to the overall current profiles obtained in the 0.3 to -0.6 V (*vs* Pt) applied potential range. Figures 1a-d show darkfield images of the same working electrode area recorded before and after application of linear sweep voltammetry (LSV) in

absence and in presence of Hg^{2+}. The intense red scattering features displayed by gold nanorods immersed in pure supporting electrolyte (1a) remained unaltered after initial LSV (1b) and after addition of Hg^{2+} into the cell (1c). Thus, no perturbation of the nanorods' environment associated with these two processes was observed. In contrast, following application of cathodic linear potential sweeps in presence of Hg^{2+}, the nanorods' scattering color dramatically transitioned from red to green (1d). Additionally, scattering spectra were recorded at several randomly selected individual nanorods before and after the application of the electrochemical step. Scattering spectra of a representative single nanorod (marked with a red circle in Figure 1a-d) are reported in Figure 1e. The initial scattering spectrum of the marked nanorod, characterized by a LSPR λ_{max} centered at 671 nm and a FWHM of 53 nm (1e, black curve), showed no significant optical changes after LSV in pure electrolyte (1e, red curve) and after addition of Hg^{2+} to the electrochemical cell (1e, green curve). The slight changes in intensities were likely caused by small changes in electron density during LSV and by the addition of mercury solution as well as the disassembly and reassembly of the cell necessary for $HgCl_2$ solution injection. However, following the application of LSV in presence of Hg^{2+} significant changes occurred in the nanorod spectrum resulting in LSPR λ_{max} blue shift of 79 nm (from 671 nm to 592 nm), an increase of FWHM of 44 nm (from 53 nm to 97 nm) and a 2.5 fold decrease in intensity compared to the original spectrum.

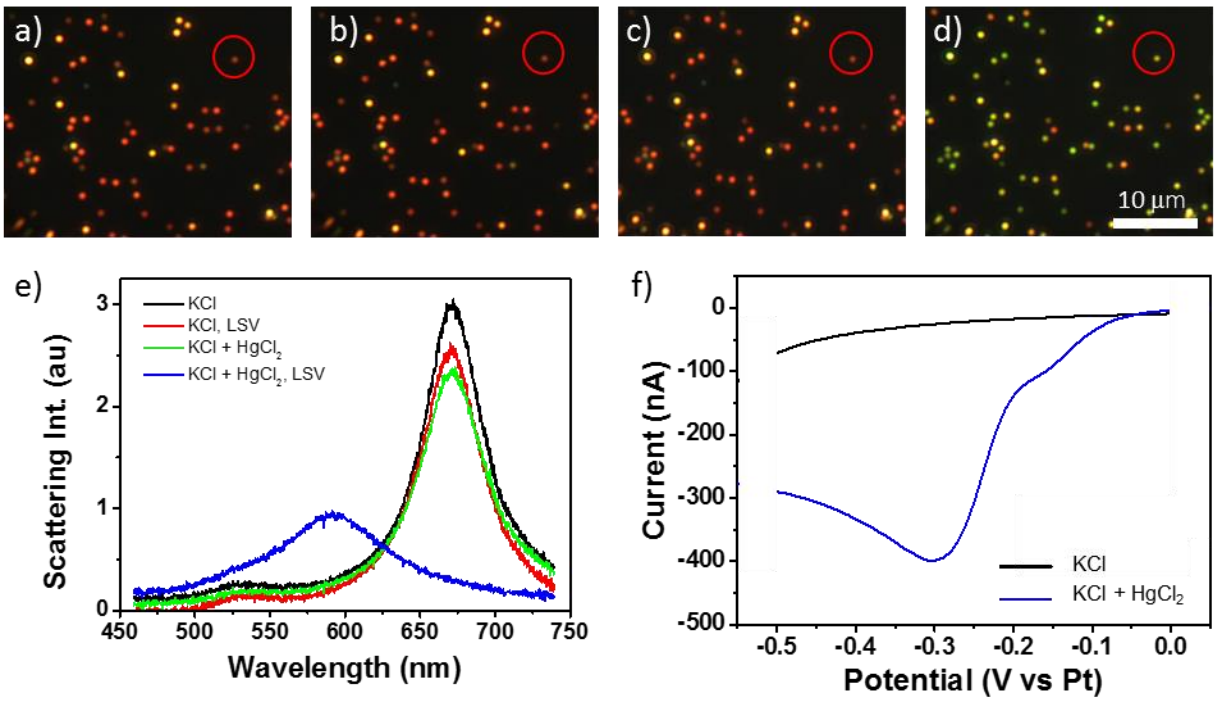

Figure 1. Darkfield images of a gold nanorod electrode immersed in a) 0.1 M KCl; b) 0.1 M KCl after LSV, c) 0.1 M KCl, 5 µM $HgCl_2$, d) 0.1 M KCl, 5 µM $HgCl_2$ after LSV; e) Scattering spectra of a representative single nanorod (marked with a red circle in a-d) before and after LSV in 0.1 M KCl and 0.1 M KCl, 5 µM $HgCl_2$; f) Linear sweep voltammograms obtained in 0.1 M KCl (black curve) and in background subtracted 0.1 M KCl, 5 µM $HgCl_2$ (blue curve). Reference electrode was Pt wire.

Corresponding linear sweep voltammograms are reported in Figure 1f. The black line is the current-voltage profile obtained in the absence of Hg^{2+}, showing no occurrence of Faradaic currents. The blue line was recorded following the addition of Hg^{2+}. The peak observed at -0.3 V was attributed to the electrochemical reduction of Hg^{2+} to Hg^0. The peak-shaped curve was characteristic of a diffusion limited behavior associated with inefficient mass transport of analyte to the electrodes. Such behavior typically occurs in closely-spaced electrodes due to limited supply of analyte to the electrodes and consequent competition for that supply between adjacent electrodes.[18-20]

The good correlation between optical and electrochemical responses strongly suggests that the recorded nanorod LSPR blue shift and the scattering color transition from red to green are associated with the reduction of Hg^{2+}. It is known from literature that the chemical reduction of Hg^{2+} in presence of metal nanoparticles causes formation of an amalgam resulting in spectral blue shifts.[14,21] LSPR blue shifts were found to be particularly strong in nanorod-shaped particles as a result of two contributions: alteration of nanorod chemical composition due to amalgam formation and consequent morphological transition from elongated to spherical shape.[22-24] This process was investigated in detail in a previous publication,[13] where nanorods exposed to 5 μM Hg^{2+} solutions showed decreased aspect ratio (from initial AR = 3 to AR = 1.6) symptomatic of the occurrence of a reshaping process, and increased volume (from initial 20,000 nm^3 to 26,000 nm^3) symptomatic of mercury incorporation (estimated mercury content of 19 atoms %). Similarly, in the present work the integration of the measured current over time yielded a charge flow of 2.72×10^{-6} C. Bringing this value in relation to the electrode nanorod density (8 nanorods/100 μm^2) yielded 1.52×10^{6} reduced mercury atoms/nanorod and a mercury:gold atom ratio of 23:77, determined on the basis of an average nanorod size of 39×76 nm. We speculate that the deposition of these reduced mercury atoms on nanoelectrodes induced morphological alterations of gold nanorods responsible for the observed spectral behavior. This point was corroborated by the observed decrease in aspect ratio of gold nanorods from the initial value of 1.9 to 1.2 following the application of linear sweep voltages in presence of $HgCl_2$ (Figure S6). In an attempt to improve analyte mass transport, a nanorod working electrode of decreased density was fabricated (1 nanorod/100 μm^2, corresponding to an inter-nanorod distance of ca. 11 μm). The nanorod density and average nanorod spacing were estimated using the same method described above for high density electrodes. Figure 2a-f show the spectroelectrochemical

response characteristic of the low density electrode towards Hg^{2+}. Scattering color transition from red to green (2a-d) accompanied by a marked LSPR blue shift (2e) and formation of a small electrochemical reduction peak (2f) occurred upon LSV in presence of 5 μM $HgCl_2$ solutions, similar to what was previously observed with the high density electrode.

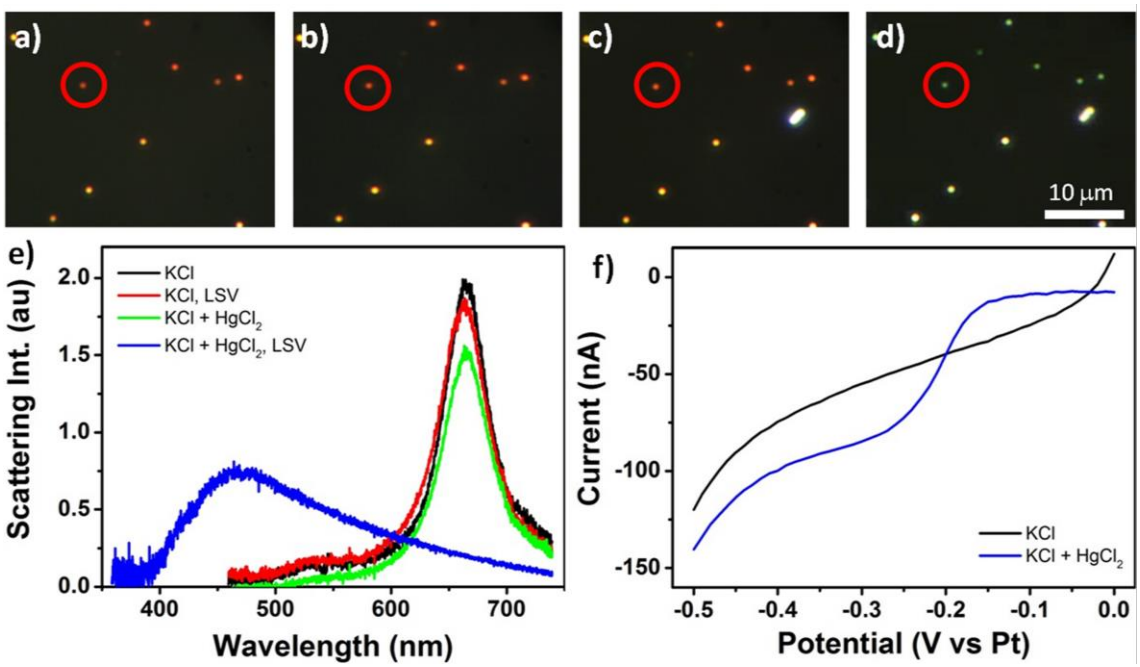

Figure 2. Darkfield images of gold nanorods a) 0.1 M KCl as deposited, b) 0.1 M KCl after LSV, c) 0.1 M KCl, 5 μM $HgCl_2$, d) 0.1 M KCl, 5 μM $HgCl_2$ after LSV; e) Scattering spectra of a representative single nanorod (marked with a red circle in a-d) before and after LSV in 0.1 M KCl and 0.1 M KCl, 5 μM $HgCl_2$; f) Voltammograms in 0.1 M KCl (black curve) and in background subtracted 0.1 M KCl, 5 μM $HgCl_2$ (blue curve). Reference electrode was Pt wire.

However, closer comparison of individual scattering spectra revealed that the nanorod circled in red (Figure 2a-d) in the lower density electrode experienced a much larger blue shift (197 nm versus 79 nm) and a much larger FWHM broadening (123 nm against 44 nm) compared to the nanorod circled in red in the higher density electrode. The calculated ratio of mercury:gold atom

generated at the low density electrode was equal to 31:69, based on the calculated charge flow (6.17×10^{-7} C) yielding a 1.6 fold increase in the number of reduced mercury atoms/nanorod (2.46×10^{6}) compared to that at the high density electrode. Such higher ratio compared to the high density electrode (23:77) was considered responsible for the larger LSPR blue shift observed at the low density electrode. Additionally, as expected due to the lower nanorod density, the overall voltammogram (Figure 2f) obtained after addition of Hg^{2+} displayed reduced current magnitudes compared to the high density electrode and displayed only a small reduction peak at -0.25 V. However, interestingly, the current-voltage profile appeared to be of sigmoidal shape, indicating an enhanced mass transport, i.e., approaching steady-state behaviour. Such behavior is typical of well-spaced electrodes, whereby the increased distance between neighboring electrodes results in reduced competition for analyte supply.[18-20] Of note, the calculated amount of Hg^{2+} reduced during one linear sweep (8.47×10^{12} ions at higher density electrodes and 1.93×10^{12} ions at lower density electrodes) was small compared to the initial amount of Hg^{2+} in solution (2.44×10^{14} ions), showing that no depletion of mercury in the solution took place during the process.

The influence of inter- nanoscale electrode distance on the shape of current-voltage signals under sweep voltammetric conditions was investigated by Wahl *et al.*[17] who observed peak-shaped responses typical of diffusion-limited behavior for closely-spaced nanoelectrodes (ca. <13 μm) and sigmoidal signals typical of steady-state behavior for increased inter-electrode distance. Accordingly, we speculate that the relatively small average distance between nanorods (~ 6 μm) at the high density ITO/nanorod electrode might have resulted in the generation of peak-shaped current profiles (Figure 1f) due to poor diffusional behavior. In contrast, the higher inter-nanorod distance (~ 11 μm) at the low density nanorod electrode probably resulted in the display of

voltammograms of sigmoidal shape (Figure 2f) typical of a transition towards steady-state behavior, likely due to improved mass transport at the electrodes.

In order to prove this hypothesis, preliminary simulations were undertaken using Comsol Multiphysics® aiming at investigating analyte concentration profiles for the reduction of mercury under linear sweep voltammetry at (i) a single gold nanorod electrode, (ii) two gold nanorod electrodes with an inter-nanorod separation of 6 μm and (iii) two gold nanorod electrodes with an inter-nanorod separation of 11 μm. Migration and convection effects were assumed to be negligible due to the chosen experimental conditions (un-agitated solutions, at constant temperature, over short time periods and in the presence of excess supporting electrolyte). The models were implemented to mirror experimental conditions: LSV in 5 μM $HgCl_2$ in 0.1 M KCl solution over a potential window of 0 V - 0.5 V (*vs* Pt) at 50 $mV.s^{-1}$ scan rate. The diffusion coefficient was set to 1.4 x 10^{-5} $cm^2.s^{-1}$.[25] An experimentally determined value of -0.3 V (*vs* Pt) was employed for E^0, the formal potential of Hg^{2+}/Hg^0. Due to the high aspect ratio of the nanorods, a simplified two dimensional model known as the diffusion domain approach was adopted. In this approach, each nanorod was modelled as a 39 nm x 76 nm rectangle located at the centre of a much larger rectangle (space domain). To ensure accuracy of the simulations, the space domain area was selected to be large enough to ensure that bulk-like conditions at the boundaries remained unaffected by electrochemical processes occurring at the electrodes. Simulations were allowed to iteratively resolve until a convergence error less than 2% was achieved.

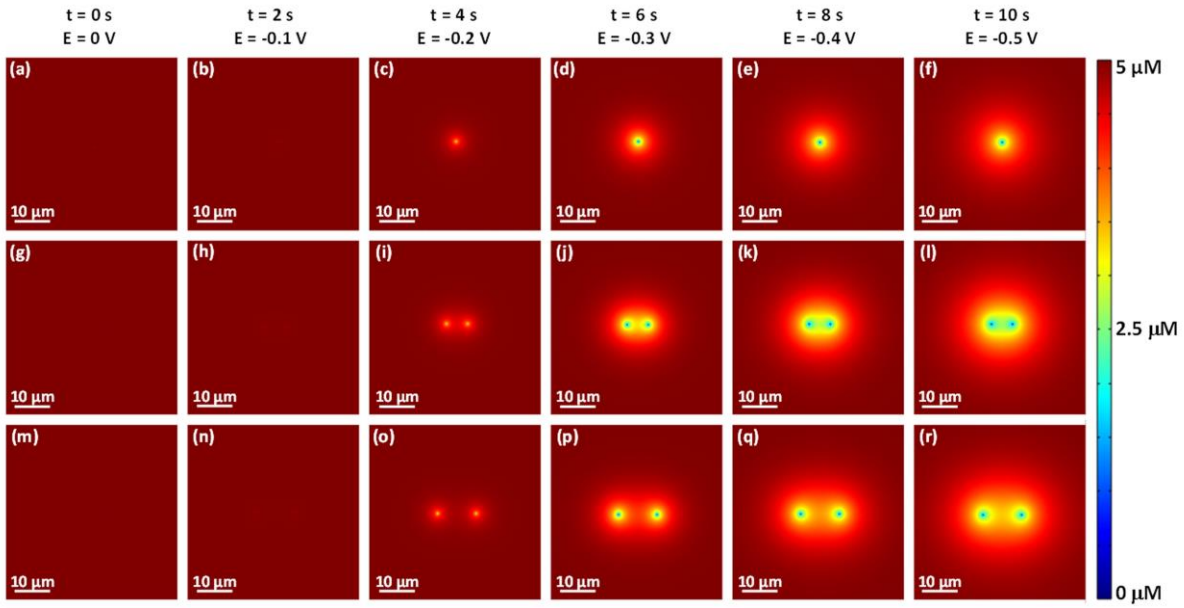

Figure 3: Top view 2D simulations of Hg^{2+} concentration profiles at different times throughout LSV measurements (at t = 0 s (start at 0 V *vs* Pt), t = 2 s, t = 4 s, t = 6 s, t = 8 s and t = 10 s (end at -0.5 V *vs* Pt)) for: a single gold nanorod electrode (a-f), two gold nanorods spaced by 6 µm (g-l) and two gold nanorods spaced by 11 µm (m-r).

For a single gold nanorod electrode (Figure 3 a-f) the diffusion layer thickness was found to be uniform (circular) and much larger than the nanorod dimensions, strongly implying that the analyte mass transport behavior was dominated by radial diffusion (i.e., steady-state behavior) throughout the whole duration of the applied LSV. Of note, at t = 6 s, when the applied potential corresponded to the strongest reduction of Hg, the extent (radius) of the diffusion layer was on the order of 5 µm. This suggests that for multiple nanorod electrodes an inter-nanorod separations of ≥ 10 µm is required to allow transition from poor diffusional behavior arising from strong overlap of adjacent diffusion profiles to enhanced diffusional behavior arising from reduced overlap. Completely independent diffusion profiles are theoretically predicted for inter-nanorod spacings ≥ 16 µm, corresponding to twice the dimension of the final diffusion layer

thickness generated in single nanorod electrodes. To support this point simulations of electrodes with inter-nanorod separation of 6 μm (Figure 3g-l) showed complete diffusional overlap of neighboring diffusion profiles throughout the whole duration of the applied LSV, particularly evident at t = 6 s. This confirmed that the relatively short inter-nanorod separation likely caused diffusion-limited behavior in agreement with the large peak-shaped response experimentally measured at the high nanorod density electrode (Figure 1f). On the other hand, for nanorod electrodes separated by 11 μm (Figure 3m-r) simulations highlighted significant decrease in diffusional overlap, especially around t = 6 s, thereby most probably confirming that the increased spacing led to improved analyte mass transport resulting in the somewhat sigmoidal response experimentally recorded at the low nanorod density electrode (Figure 2f).

Finally, direct observation of the evolution of the amalgamation process was performed by recording real time spectra of single nanorods in presence of Hg^{2+} while the applied potential was initially held constant followed by the application of linear cathodic potential sweeps and open cell potential (ocp) conditions. Figure 4a shows a representative potential *vs* time and current *vs* time curves correlated with a 2 dimensional (2D) plot of scattering spectra recorded every second for 300 seconds for a single nanorod immersed in 0.1 M KCl, 2 μM $HgCl_2$ solution and subjected to electrochemical measurements (linear sweep voltammetry). The real time analysis of the process (Figure 4b) revealed that the nanorod LSPR λ_{max} (661 nm) remained constant during the first 30 s as the applied potential was held at 0 V (vs. Pt), then it increased slightly between 30 s and 40 s as the applied potential was held at 0.3 V (vs. Pt), and finally it strongly blue shifted between 40 s and 60 s (634 nm) as the potential was scanned linearly from 0.3 to -0.6 V (vs. Pt). The spectral intensity decreased and FWHM increased, concomitantly with the recorded blue shift arising from the application of a cathodic potential scan.

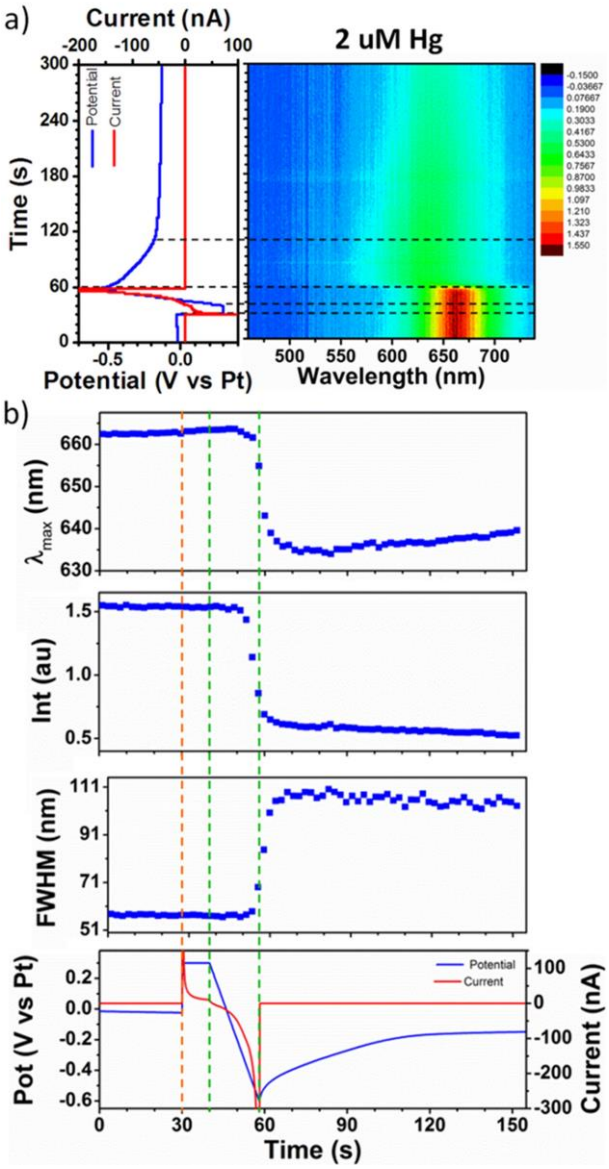

Figure 4. a) Potential *vs* time and current *vs* time curves correlated with a 2D plot of 300 scattering spectra recorded in-situ at a single representative nanorod in 0.1 M KCl, 2 µM $HgCl_2$ while the applied potential was initially held at 0 V (vs. Pt), then 0.3 V (vs. Pt), followed by the application of linear cathodic potential sweeps from 0.3 to -0.6 V (vs. Pt) and finally open cell potential conditions; b) λ_{max}, peak intensity and FWHM values extracted from Lorentzian fits to spectral data correlated with potential vs. time and current vs. time curves recorded during LSV.

According to such experimental observations and previously reported theoretical calculations,[13] the large spectral changes were associated with the deposition of mercury on the nanorod surface with formation of a core-shell structure which promoted partial dissolution of gold atoms into the shell and their diffusion leading to a spheriodization of the initial rod shape. Furthermore, as presented in Figure 4b, the nanorod optical changes were also monitored immediately after the linear sweep was carried out (i.e., under ocp conditions) for additional 242 s. It was found that the FWHM did not undergo further changes and the spectral intensity continued to drop slowly, possibly due to the nanorod moving out of focus. However, interestingly, while a large blue shift of the LSPR λ_{max} (from 664 to 634 nm) occurred at 70s, a progressive small red shift of λ_{max} to 639 nm was recorded in the following 80 s (between 70 s and 150 s). A number of processes were considered to explain the cause of the observed λ_{max} red shift: (i) oxidation of deposited mercury from the nanorods back into the solution triggered by the gradual decrease of potential from -0.6 back to 0 V; (ii) dissolution of reduced elemental mercury; (iii) diffusion of mercury away from the nanorods; (iv) diffusion of mercury into the nanorods. Oxidation of deposited mercury was considered unlikely as LSV scans in the anodic potential direction (from - 0.6 V to 0.3 V *vs* Pt) in 5 μM $HgCl_2$ solutions did not show formation of a corresponding oxidation peak (data not shown). Dissolution of mercury into the solution could occur as the solubility of mercury in water is 300 nM at 298.15 K.[25] Mercury diffusion away from the nanorods, was considered unlikely due to the extremely high affinity between gold and mercury. Diffusion of mercury into gold nanorod lattices was previously observed following chemical reduction of Hg^{2+} solutions on gold nanorods. Specifically, we have previously shown that diffusion of reduced mercury deeper into the nanorod lattices occurred at slow timescales resulting in red shifts of gold nanostructures' optical signatures measured for up to 50 h after mercury deposition

was performed.[13] Therefore, real time observation of the amalgamation process further confirmed our previously proposed mechanism for nanoscale gold-mercury amalgamation, consisting on fast deposition of reduced mercury on nanorod surfaces followed by slow diffusion of mercury into the nanorod lattices.

Alternatively, direct observation of the amalgamation process was carried out by recording real time spectra at single nanorods in presence of Hg^{2+} during ocp conditions followed by the application of chronoamperometry (CA) and finally ocp again; the ocp was monitored for 30 s before the potential was set to -0.3 V (vs. Pt) for 60 s, corresponding to the potential at which the reduction of Hg^{2+} was previously observed (Figures 1f, 2f) and subsequently the ocp was monitored for further 200 s. The electrochemical response correlated with a 2D plot of scattering spectra recorded every second for 290 seconds at a single nanorod immersed in 0.1 M KCl, 2 μM $HgCl_2$ solution and subjected to ocp-CA-ocp at a representative single nanorod is shown in Figure 5a. Detailed real-time measurements are presented in Figure 5b. During the first 30 s (i.e., under ocp conditions) the nanorod LSPR λ_{max} stayed constant (676 nm). It then gradually blue shifted to 513 nm during the application of -0.3 V potential for 60 s. Specifically an abrupt blue shift of ca. 100 nm occurred in the first 10 s of CA application (40 s in the time scale of Figure 5b), followed by a slower blue shift and formation of a plateau at 513 nm in the following 50 s (90 s in the time scale of Figure 5b). Concomitantly, spectral intensity sharply decreased during the first 10 s upon -0.3 V was applied and then remained constant. Spectral FWHMs also increased dramatically from 26 nm to 150 nm during the first 10 s of CA application and continued to grow to 315 nm in the remaining 50 s of CA application. No further changes in λ_{max}, spectral intensity and FWHM were recorded during the subsequent ocp period (first 30 s of

which are shown as section 90 s – 120 s in the time scale of Figure 5b), thereby highlighting the high stability of the process.

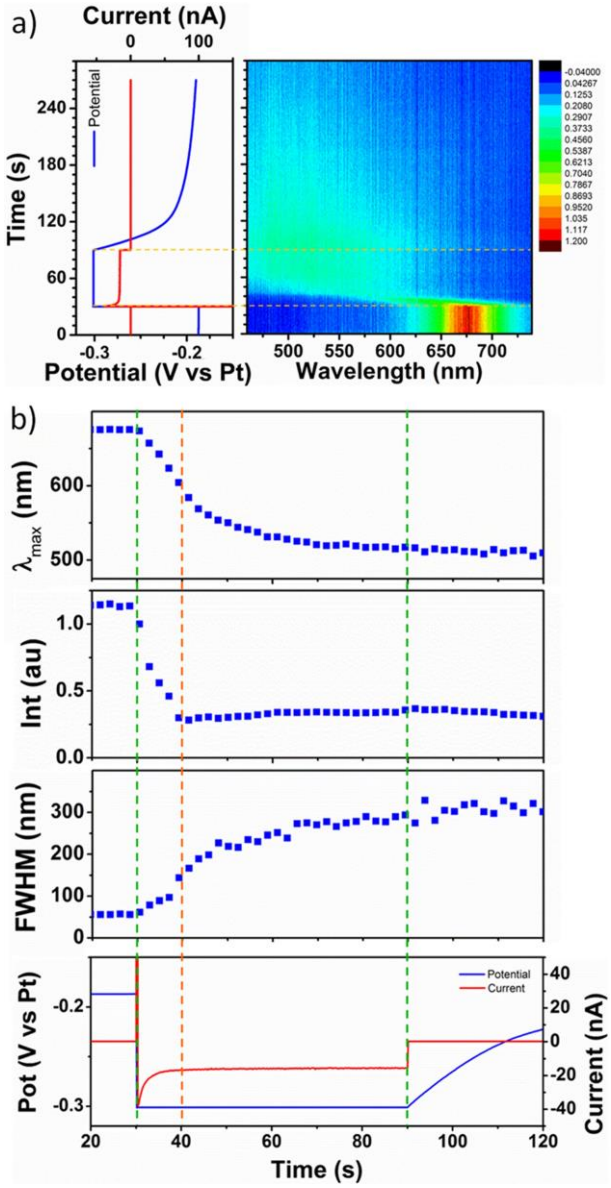

Figure 5. a) Potential vs. time and current vs. time curves correlated with a 2D plot of 290 single nanorod scattering spectra recorded in-situ at a single representative nanorod in 0.1 M KCl, 2 µM $HgCl_2$ under ocp followed by CA at -0.3 V (vs. Pt) and ocp again; b) λ_{max}, peak intensity and FWHM values extracted from Lorentzian fits to spectral data correlated with potential and current curves recorded during CA.

Under the same electrolyte/analyte concentration, CA real time measurements compared to real time LSV were characterized by a much stronger optical blue shift (163 nm compared to 27 nm) which critically remained stable upon the application of ocp conditions. In contrast to LSV, CA real-time measurements were performed by maintaining the electrode at the Hg^{2+} reduction potential for 60 s. Thus it is clear that CA real-time measurements allowed for the reduction of a much larger amount of Hg^{2+}, which in turn resulted in a stronger optical blue shift and much greater stability of λ_{max}. Consequently, a much stronger blue shift combined with significantly improved signal stability suggest that real time spectroelectrochemical measurements employing CA could be amenable to sensitive and fast detection of mercury in solution even for ultra-low concentrations of mercury (down to nM).

Conclusions

In conclusion, the process of amalgamation at nanoscale was investigated for the first time by use of a spectroelectrochemical method. This approach allowed simultaneous monitoring of optical and electrochemical responses generated at gold nanorod working electrodes upon electrochemical reduction of Hg^{2+}. The optical response of single nanorods was monitored by darkfield microscopy and showed intense scattering color transitions and marked spectral blue shifts up to 197 nm associated with amalgam formation and consequent nanorod shape transition to spherical particles. Experiments with substrates of different nanorod density indicated that larger optical blue shifts (i.e. higher sensitivity) were achieved with low nanorod density working electrodes as their large inter-nanorod spacing enabled improved analyte mass transport (observed experimentally and supported by simulations) yielding higher mercury:gold atom

ratio. Finally, direct observation of the amalgamation process was performed by recording spectral changes of one single nanorod during applied potential by both LSV and CA. Both methods delivered large information outputs, useful for elucidation of the mechanisms associated with mercury reduction at the nanoscale. Compared to LSV measurements, CA measurement gave larger optical shifts and permanent optical response in the time scale of the applied potential, suggesting that this technology could be implemented for the generation of novel electrochemical sensors for environmental and biosensing applications. The method could also be extended to detection of other plasmonic metals such as copper, silver and aluminum and has the potential for multi-analyte detection of plasmonic metals displaying distinct reduction peaks and associated plasmonic responses.

ASSOCIATED CONTENT

AUTHOR INFORMATION

Corresponding Author

Daniela Iacopino, Tyndall National Institute, Dyke Parade, Cork, Ireland, phone: 00353 (0)21 2346182, email: daniela.iacopino@tyndall.ie

Author Contributions

The manuscript was written through contributions of all authors. All authors have given approval to the final version of the manuscript.

ACKNOWLEDGMENTS

This work was supported by the European Union Seventh Framework Programme (project 263091 Hysens and 312829 Rosfen).

Supporting Information. Design of spectroelectrochemical cell, gold nanorod/ITO electrode characterization, electrochemical curves of Hg^{2+} reduction on gold nanorod /ITO electrodes, SEM imaging of gold nanorod/ITO electrode following Hg(II) reduction. This material is available free of charge via the Internet at http://pubs.acs.org.

REFERENCES

(1) Raschke, G.; Kowarik, S.; Franzl, T.; Sönnichsen, C.; Klar, T. A.; Feldmann, J.; Nichtl A; Kürzinger, K. Biomolecular recognition based on single gold nanoparticle light scattering. *Nano Lett.*, **2003**, *3*, 935–938.

(2) Shi, L.; Jing, C.; Ma, W.; Li, D.-W.; Halls, J. E.; Marken F.; Long, Y.-T. Plasmon resonance scattering spectroscopy at the single-nanoparticle level: real-time monitoring of a click reaction. *Angew. Chem*. *Intern. Ed.,* **2013**, *52*, 6011 –6014.

(3) Buurmans L. C.; Weckhuysen B. M. Heterogeneities of individual catalyst particles in space and time as monitored by spectroscopy. *Nat. Chem*., **2012**, *4*, 873–886.

(4) Liu Y.; Huang, C. Z. Real-time dark-field scattering microscopic monitoring of the in situ growth of single Ag@Hg nanoalloys. *ACS Nano*, **2013**, *7*, 11026-11034.

(5) . Klar, T. A.; Perner, M.; Grosse, S.; Von Plessen, G.; Spirkl W.; Feldmann, Surface-plasmon resonances in single metallic nanoparticles. J. *Phys. Rev. Lett*., **1998**, *80*, 4249 4252.

(6) Schultz, S.; Smith, R. D.; Mock, J. J.; Schultz, D. A. Single-target molecule detection with nonbleaching multicolor optical immunolabels. *Proc. Natl. Acad. Sci. U.S.A.*, **2000**, *97*, 996-1001.

(7) Novo, C.; Funston A. M.; Mulvaney, P. Direct observation of chemical reactions on single gold nanocrystals using surface plasmon spectroscopy. *Nat. Nanotech*., **2008**, *3*, 598-602.

(8) Novo, C.; Funston, A. M.; Gooding A. K.; Mulvaney, P. Electrochemical charging of cingle gold nanorods. *J. Amer. Chem. Soc*., **2009**, *131*, 14664- 14666.

(9) Chapman R.; Mulvaney, P. Electro-optical shifts in silver nanoparticle films. *Chem. Phys. Lett*., **2001**, *349*, 358-362.

(10) Ung, T.; Giersig, M.; Dunstan D.; Mulvaney, P. Spectroelectrochemistry of colloidal silver. *Langmuir*, **1997**, *13*, 1773-1782.

(11) Chirea, M.; Collins, S. S.; Wei X.; Mulvaney, P. Spectroelectrochemistry of silver deposition on single gold nanocrystals. *Phys. Chem. Lett.*, **2014**, *5*, 4331-4335.

(12) Byers, C. P.; Zhang, H.; Swearer, D. F.; Yorulmaz, M.; Hoerner, B. S.; Huang, D.; Hoggard, A.; Chang, W.-S.; Mulvaney, P.; Ringe, E. et al. From tunable core-shell nanoparticles to plasmonic drawbridges: Active control of nanoparticle optical properties. *Sci. Adv.*, **2015**, 1, e1500988.

(13) Schopf, C.; Martín, A.; Schmidt M.; Iacopino, D. Investigation of Au–Hg amalgam formation on substrate-immobilized individual Au nanorods. *J. Mater. Chem. C*, **2015**, *3*, 8865-8872.

(14) Ojea-Jiménez, I.; López, X.; Arbiol J.; Puntes, V. Citrate-coated gold nanoparticles as smart scavengers for mercury(II) removal from polluted waters. *ACS Nano*, **2012**, *6*, 2253-2260.

(15) Qian, H.; Pretzer, L. A.; Velazquez, J. C.; Zhao Z.; Wong, M. S. Gold nanoparticles for cleaning contaminated water. *J. Chem. Tech. Biot. B*, **2013**, *88*, 735-741.

(16) Alvarez-Puebla, R. A.; Agarwal, A.; Manna, P.; Khanal, B. P.; Aldeanueva-Potel, P.; Carbo-Argibay, E.; Pazos-Perez, N.; Vigderman, L.; Zubarev, E. R.; Kotov N. A. et al. Gold nanorods 3D-supercrystals as surface enhanced Raman scattering spectroscopy

substrates for the rapid detection of scrambled prions. *Proc. Natl. Acad. Sci. U. S. A*., 2011, *108*, 8157-8161.

(17) Wahl, A.; Dawson, K.; MacHale, J.; Barry, S.; Quinn, A.J.; O'Riordan, A. Gold nanowire electrodes in array: simulation study and experiments. *Faraday Discuss.*, **2013**, *164*, 377-390.

(18) Rees N. V.; Compton, R. G. Voltammetry as a probe of displacement. *Chem. Comm*., **2010**, *46*, 4238-4248.

(19) Davies T. J.; Banks, C. E.; Compton, R. G. Voltammetry at spatially heterogeneous electrodes. *J. Sol. State Electrochem*., **2005**, *9*, 785-808.

(20) Dawson, K.; Wahl, A.; Pescaglini, A.; Iacopino, D.; O'Riordan, A. Electroanalysis at ultramicro and nanoscale electrodes: a comparative study. J. *Electrochem. Soc*., **2014**, *161*, B3055-B3050.

(21) Bootharaju, M. S.; Chaudhari K.; Pradeep, T. Real time plasmonic spectroscopy of the interaction of Hg^{2+} with single noble metal nanoparticles. *RSC Adv*., **2012**, *2*, 10048-10056.

(22) Rex, M.; Hernandez F. E.; Campiglia, A. D. Pushing the limits of mercury sensors with gold nanorods. *Anal. Chem*., **2005**, *78*, 445-451.

(23) Chemnasiri W.; Hernandez, F. E. *Sens. Act. B*, **2012**, *173*, 322-328.

(24) Trieu, I.; Heider, E. C.; Brooks, S. C.; Campiglia, A. D. Gold nanorods for surface plasmon resonance detection of mercury (II) in flow injection analysis. *Talanta,* **2014**, *128*, 196-202.

(25) Kuss, J.; Holzmann, J.; Ludwig, R. An elemental mercury diffusion coefficient for natural waters determined by molecular dynamics simulations. *Environ. Sci. Technol*., **2009**, *43,* 3183–3186.

(26) Clever, H. L.; Johnson S. A.; Derrick. M. E. The solubility of mercury and some sparingly soluble mercury salts in water and aqueous electrolyte solutions. *J. Phys. Chem.*, **1985**, *14*, 631-680.

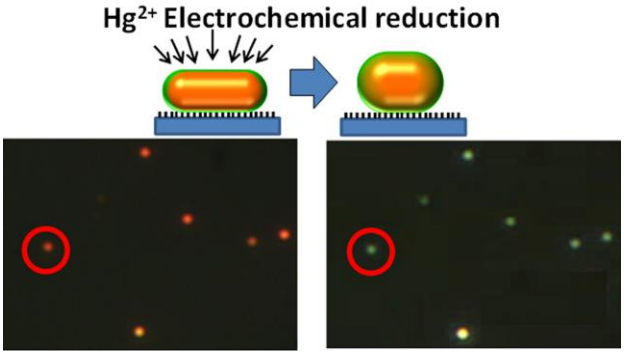

TOC graphic